

DETAILED SUMER OBSERVATIONS OF CORONAL LOOP FOOTPOINT DYNAMICS

SCOTT W. McINTOSH

Universities Space Research Association, Cooperative Program in Space Sciences, Seabrook, MD 20706; and Laboratory for Astronomy and Solar Physics,
NASA Goddard Space Flight Center, Greenbelt, MD 20771; scott@grace.nascom.nasa.gov

AND

ARTHUR I. POLAND

Laboratory for Astronomy and Solar Physics, NASA Goddard Space Flight Center, Greenbelt, MD 20771; and School of Computational Science,
George Mason University, Fairfax, VA 22030; apoland@scs.gmu.edu

Received 2003 June 5; accepted 2003 December 3

ABSTRACT

For the most part, the characteristics of heating in the open corona and in closed coronal loops are determined by observing the emitted plasma intensity as a function of position and comparing this with model calculations. There are also some efforts that include observed velocity and still others that use theoretical physical processes such as electrodynamic or turbulent heating, for example. With a view toward future modeling endeavors, we investigate the temporal behavior of the intensity and velocity of a magnetic loop footpoint as observed by SUMER on the *Solar and Heliospheric Observatory (SOHO)* spacecraft as part of *SOHO/TRACE* Joint Observing Program 72. We study these quantities in emission lines that were specifically chosen to span the temperature domain of the upper chromospheric and transition region plasmas (10^5 – 10^6 K). We discuss the implications of these observations, suggest improvements, and present some new avenues of exploration. The most significant result is the demonstration of the importance of including the measurement of velocity as a function of time in the loop footpoint region.

Subject headings: Sun: atmospheric motions — Sun: magnetic fields — Sun: transition region —
Sun: UV radiation

On-line material: color figures

1. INTRODUCTION

The study of the magnetic loops that ubiquitously permeate the outer solar atmosphere is critical if we are to understand the coronal heating process and the flow of mass and energy through this region. The primary question can be simply stated as, “What is the energy source for loops in the solar atmosphere, and how is their structure sustained?” The best approach to answering this complex coupled question has been to observe quantities that lead to the derivation of temperature, density, and Doppler velocity distributions in these loops and to attempt to match observed values with the results from models using the equations of conservation of mass, momentum, and energy. In theory, the only unknown left in finding the solution to these equations is the energy input. This topic has received a great deal of attention from the community in recent years, especially following the launch of the *Solar and Heliospheric Observatory (SOHO)*; Fleck, Domingo, & Poland 1995) and *Transition Region and Coronal Explorer (TRACE)*; Handy et al. 1999) missions and has been the subject of several dedicated workshops (see, e.g., Vial & Kaldeich-Schürmann 1999; Engvold et al. 2000, 2001).

Despite the many observational data sets and theoretical models of loops in the solar atmosphere, we still understand remarkably little about the underlying physics of their motions, mass balance, and energy source. Much of the reason for this “information gap” arises from the fact that we cannot directly measure these plasma quantities in situ and must rely on their inference, or inversion, from the observed electromagnetic radiation. Such inferences, from remotely sensed data, are often not straightforward and are fraught with a large

degree of non-uniqueness (see, e.g., Craig & Brown 1986; Judge & McIntosh 1999). Indeed, when they have been observed, the spatial and temporal variation has been discarded by taking the spatial and temporal averages that were needed for the information to be incorporated into models (see Mariska 1992). On an instrumental level, we have also lacked the means to provide the quality of observations needed to adequately provide the quantitative loop information with sufficient accuracy. Ideally, what we need are observations with sufficient resolution in time and space, such that we can accurately derive the primary quantities of temperature, density, and velocity as functions of time and space. These quantities would then be applied directly as inputs to physical models to verify our understanding of what is observed and allow us to deduce the full energy input distribution. Indeed, several investigations are already in development (see, e.g., Sakai & Furusawa 2002 and Petrie et al. 2003, among others).

In this paper we present measurements that will provide improved loop model inputs. These measurements were obtained through the analysis of data from the Solar Ultraviolet Measurement of Emitted Radiation (SUMER; Wilhelm et al. 1995) instrument of *SOHO* and *TRACE* EUV data taken on 1998 May 17 (14:30–16:00 UT). In § 2 we demonstrate that the spatial and temporal averaging of quantities is not an accurate measure for any observation or computational loop model. By studying the temporal variation of observed line intensities and velocities, we demonstrate that the time-averaged picture is not sufficient and that velocities vary on most temporal scales. We conclude, in § 3, that the application of time-resolved quantities as boundary conditions and “observables” in model calculations is essential because

velocities show variations that are not always apparent in intensities.

2. DATA REDUCTION AND ANALYSIS

To measure the temperature, density, and velocity of the footpoint of a magnetic loop, we must follow several steps. First we must identify the footpoint of a loop along the *SOHO* SUMER slit. We must observe a sufficient number of spectral lines so that we can deduce the temperature and density distribution. Finally, we must have observations of sufficiently high temporal resolution that we are not implicitly removing temporal variations. We have identified a data set that satisfies these criteria as part of the *SOHO/TRACE* Joint Observing Program (JOP) 72 outlined in Judge, Tarbell, & Wilhelm (2001). This joint *TRACE* and SUMER data set consists of *TRACE* UV/EUV observations and a SUMER time series of five principal spectral lines just to the southeast of NOAA active region 8222 on 1998 May 17 over a period of 1.5 hr (see Table 1, and for details of the observed lines and further detail on the joint observing program, see Judge et al. 2001). These high spatial ($1'' \times 120''$ slit) and temporal resolution (12.5 s cadence) SUMER spectral time series were specifically chosen to span the 10^5 – 10^6 K temperature range of the highly dynamic upper chromosphere and transition region. The principal¹ lines chosen are N III ($\lambda 764$), N IV ($\lambda 765$), O IV ($\lambda 787$), O V ($\lambda 760$), and the Ne VIII $\lambda\lambda 770, 780$ line pair.

Unfortunately, this instance of JOP 72 did not allow for a high-cadence 171/195 Å *TRACE* study, instead opting for the 1700, 1600, and 1550 Å chromospheric time series. As a result, the only 171/195 Å coronal images taken were in pairs at the start and end of the SUMER sequence, thus only providing us with context images. Figure 1 provides the EUV coronal context for this data set, in which we show the *TRACE* 171 Å bandpass image taken at the start of the SUMER time series. Careful co-alignment of the Ne VIII $\lambda 770$ line intensities along the SUMER slit with the *TRACE* 171 Å context images (and the derived *TRACE* “C IV” $\lambda 1550$ image time series) provided a SUMER slit position (*center*) of ($x = -33''$, $y = 390''$). There are two separate physical regions along the SUMER slit. It is clear that the region with $y < 60$ is influenced by

¹ There are several spectral windows where there are secondary lines; N III $\lambda 764$ is one (see Fig.2). Likewise, there are three more O V lines in the window of O V $\lambda 760$, and there is an O IV blend in the blue wing of the Ne VIII $\lambda 780$ line. Such blends are accounted for in the presented analysis. If a duplicate of an ion exists, then its variability is only reported if it differs significantly from the line that is a spectral window principal ion.

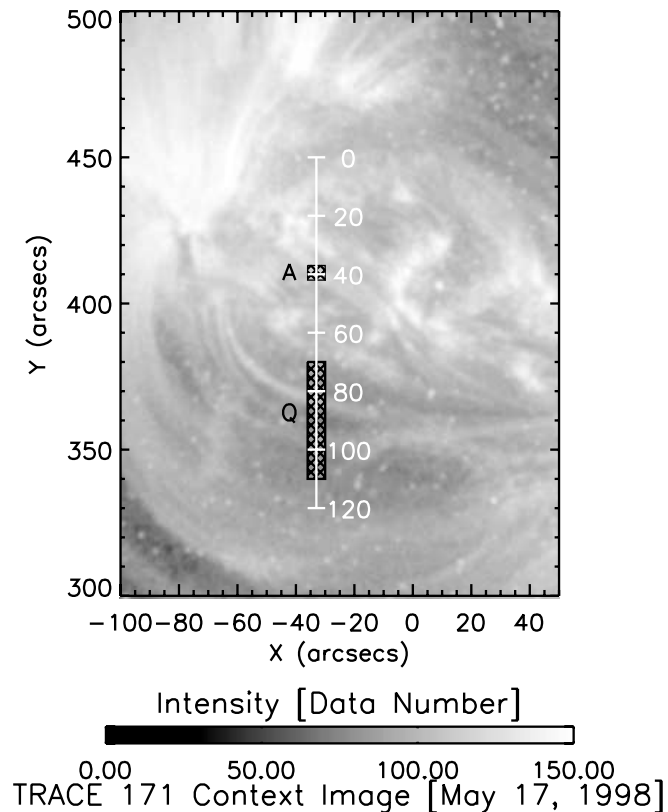


FIG. 1.—Location of the *SOHO* SUMER slit and the regions, along that slit, that we use to study the loop footpoint velocities and intensities. The loop footpoint, region A, is shown about position 40, and the quiet-Sun reference region, region Q, is also shown. This image provides context for the observations made here.

the active region, while the region with $y > 60$ is essentially quiet. Considering Figure 1 and the simultaneously obtained SUMER line profiles, we note the position of a loop footpoint at the location (position $y = 40 \pm 1$). In Figure 1 this point is centered on the small, black, cross-hatched box labeled A. Hereafter, we refer to region A as our footpoint. We have also marked a non-footpoint quiet-Sun control region as region Q (the cross-hatched region $70 < y < 110$). Region Q will be used as a calibration source for observed Doppler shifts in region A, as explained below.

The SUMER data require significant processing to permit quantitative analysis. IDL programs to perform these tasks are

TABLE 1
DETAILS OF OBSERVATIONS FROM THE FOOTPOINT REGION (A) AND THE AVERAGED REGION Q AS INDICATED IN FIGURE 1

Ion	T_e^*	λ	$D(\lambda)$ (mÅ pixel ⁻¹)	$\langle P_Q \rangle$ (Å)	σP_Q (pixels)	V_C	$\langle I_Q \rangle$ (ergs cm ⁻² s ⁻¹ sr ⁻¹)	$\langle P_A \rangle$ (Å)	σP_A (pixels)	$\langle V_A \rangle$ (km s ⁻¹)	$\langle I_A \rangle$ (ergs cm ⁻² s ⁻¹ sr ⁻¹)
N III.....	4.95	764.34	0.04467	764.35	0.10	-5.1	3.99	764.36	0.25	-8.27	4.30
N IV.....	5.12	765.14	0.04467	765.17	0.12	-11.0	33.78	765.21	0.40	-27.52	120.69
O IV.....	5.16	787.16	0.04461	787.19	0.14	-11.0	17.05	787.24	0.38	-28.92	173.97
O V.....	5.34	760.23	0.04469	760.26	0.12	-10.6	35.10	760.32	0.38	-34.27	43.99
Ne VIII.....	5.76	770.10	0.04466	770.11	0.10	-5.3	78.03	770.12	0.26	-7.58	295.51
Ne VIII.....	5.76	780.23	0.04463	780.24	0.10	-5.3	37.97	780.25	0.27	-7.97	163.65

NOTES.—We show the ion, the temperature of maximum line emissivity (T_e^* log K), the wavelength λ , the spectral dispersion of SUMER in that window [$D(\lambda)$], the mean center positions ($\langle P_X \rangle$) of the Gaussian line profile, their deviation (σP_X), the mean velocity ($\langle V_X \rangle$) and the mean integrated line intensity ($\langle I_X \rangle$) in region X (i.e., A or Q). We also provide V_C , the quiet-Sun Doppler velocity derived by Chae et al. (1998a). Other than N III, all of these lines are the principal lines in each of the SUMER spectral windows.

generally available, with documentation, on the *SOHO* Web site² (see, e.g., Teriaca 2001). Following flat-field, geometric, and radiometric (for absolute intensity measurements) corrections, we are in a position to fit line profiles to the 50 pixel-wide SUMER spectral windows. To fit the line profiles in a robust and accurate manner, we have chosen to use the genetic algorithm (GA) method that was outlined in McIntosh et al. (1998). While we fitted the line profiles at full temporal resolution for regions A and Q, we have binned the 3 spatial pixels in region A and 40 pixels in region Q in order to raise the signal-to-noise level for each profile fit. As an example, Figure 2 shows the spectral window of the N III/N IV line pair in regions A (*top*) and Q (*bottom*) with their GA fits (*solid thick lines*), their rest position (from the data header; *solid gray line*), and the measured line positions with dash-dotted and dashed lines, respectively, at one particular point in the time series. The systematic offset of the quiet-Sun redshift and the further subsequent footpoint redshift are clear, as is the variation in the line shifts with temperature.

The absolute velocity in region A is calculated by using the line positions from region Q (P_Q) as a reference, either as an average over time or as a function of time (we see that there is little difference). The “normal” line position at any time t in region Q is assumed to have the accepted quiet-Sun Doppler shift, V_C , of Chae, Schüle, & Lemaire (1998a; Chae, Yun, & Poland 1998b). The true velocity in region A is then determined by the deviation of the line position at A from that at Q. That is,

$$P_A(t) = P_Q(t) + \delta P_C, \quad (1)$$

where δP_C is the calculated difference between the Q line position and the additional line shift from V_C . In this way $P_A(t)$ is an estimate of the absolute Doppler shift of the line in the footpoint of region A as a function of time, with the accuracy based on our assumption of knowing the velocity in region Q. In this way our measurement is not dependent on knowledge of the absolute quiet-Sun line position (cf. Dammasch et al. 1999). In Table 1 we present details of the

² See <http://sohowww.gsfc.nasa.gov>.

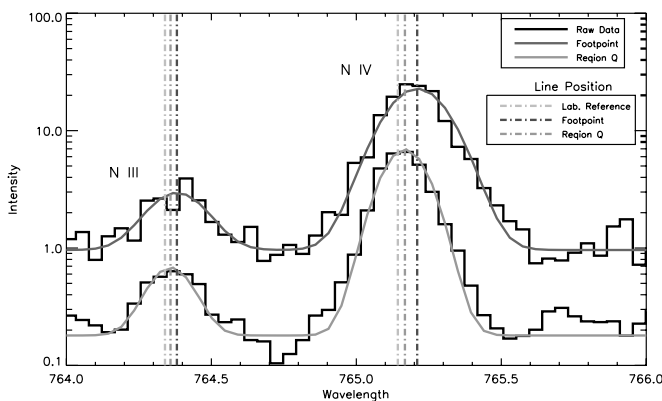


FIG. 2.—Data from the SUMER spectral window around 765 Å for regions A and Q containing the N III emission line at 764.36 Å and N IV line at 765.14 Å some 40 minutes into the time series. We mark the rest positions of each line by solid gray vertical lines. We show the GA fitted line profiles and the line positions from regions A and Q, marked by dashed and dash-dotted lines, respectively.

observed emission lines, the average and deviations of the Doppler shift (in pixels) in regions Q and A, and the mean region A Doppler velocity and intensity. We note that the typical error introduced in the derivation of $P_A(t)$, and hence $V_A(t)$ from the deviation of $P_Q(t)$, is on the order $\sim \pm 4 \text{ km s}^{-1}$.

In Figure 3 we present the intensity and velocity variations for all of the observed lines of the footpoint (region A) over the duration of the SUMER time series. While the bottom (intensity) panels of the figure are identical, the top (Doppler velocity) panels show the results for the two calibration methods applied to the line positions, where we take the time average of P_Q (*left*) and where we account for the full temporal variation in P_Q (*right*). There are several points to note in examining these panels.

1. The difference between using average velocities in region Q and time-varying values is sufficiently small that we need only consider one set of data.
2. In the intensity plot it can be seen that there are well-correlated intensity variations for the three lines formed at temperatures below 500,000 K, while there seem to be no real variations for the hotter Ne VIII lines ($T_e \sim 700,000 \text{ K}$), except for three distinct points at 30, 53, and 68 minutes, where intensity maxima occur across all temperatures but are especially pronounced in the cool lines. These intensity maxima occur in the high-temperature lines when the Doppler shifts are strongest. Such strong intensity enhancements have recently been shown to be directly correlated to large downflows in small, highly concentrated magnetic flux regions (Cadavid et al. 2003). This fact may provide additional evidence that region A is indeed the location of a magnetic loop footpoint.
3. The velocities are grouped such that the coolest and hottest lines have nearly the same velocity, in agreement with the quiet-Sun velocity “bell” curve of Chae et al. (1998a), where the velocity has a maximum in the $2 \times 10^5 \text{ K}$ range and is lower near 80,000 K and $8 \times 10^5 \text{ K}$.
4. The velocities near $2 \times 10^5 \text{ K}$ are much higher than quiet-Sun values (-30 vs. -10 km s^{-1}), whereas the velocities at the lower and highest temperatures are closer to quiet-Sun values (-5 to -10 vs. -5 km s^{-1}).
5. There are many time variations in velocity at all temperatures with cycle times that vary from less than a minute to approximately 20 minutes, and they seem to be well correlated in time.

In Figure 4 we show a sample correlation scatter plot for the mean subtracted intensities (*light diamonds*) and velocities (*dark diamonds*) of the N IV–Ne VIII $\lambda 770$ lines. We can see that the velocities are well correlated (coefficient 0.53), while the intensities are not (coefficient 0.24). The correlation coefficients for all line combinations (compared to the Ne VIII $\lambda 770$ line) are given in Table 2. Closer inspection of the velocity variations in region A (and the quantities of Table 2) show that there are small, near negligible, delays between the “cool” lines (N III, O IV, N IV, and O V) and the hotter Ne VIII pair. It is interesting to note that these delays are consistent with the assumption that the height difference between the two temperatures is what one would expect from most models with the propagation speed being the speed of sound. Variations of this type are not observed in the quiet region Q; there is substantially less variation in the intensities or velocities as demonstrated in Table 1, and any variation can most likely be attributed to instrumental effects or solar noise. It is fair to say that there is no real, characteristic, long-duration frequency or

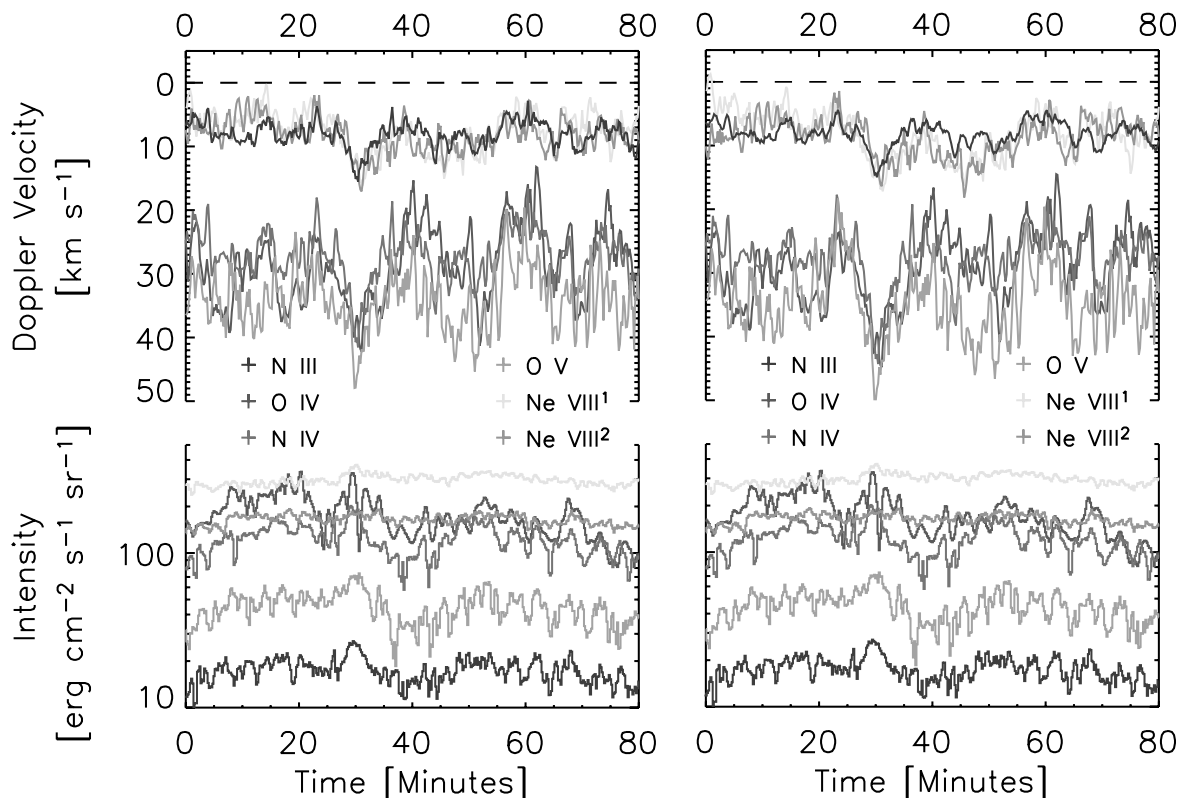


FIG. 3.—Time series evolution of the velocities (*upper panels*) and intensities (*lower panels*) for the footpoint, region A of Fig. 1. We see that there is a great deal of correlated variation across the five lines from the Doppler Shifts in the loop footpoint. There appears to be a disconnect in this correlation, for the line intensities, between the cool (N III, N IV, O IV, and O V) and hot (Ne VIII $\lambda\lambda 770, 780$) lines. [See the electronic edition of the Journal for a color version of this figure.]

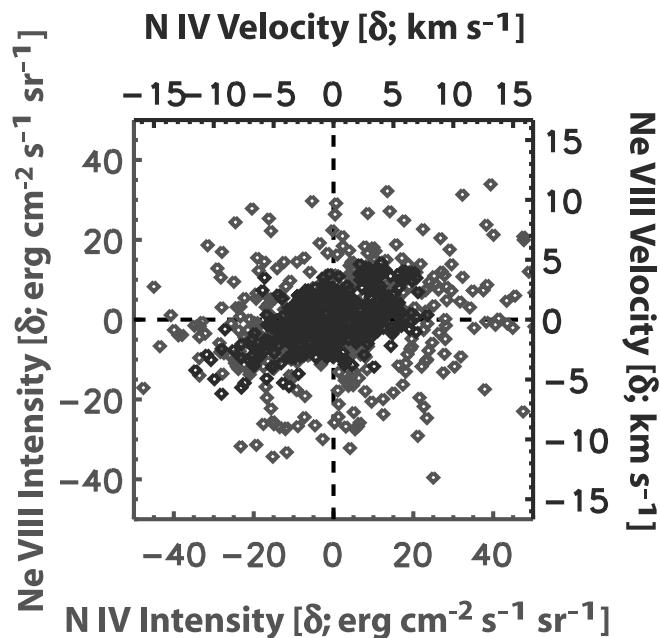


FIG. 4.—Sample scatter correlation plots between the N IV and Ne VIII ($\lambda 770$) line mean-subtracted intensities (*light diamonds*) and Doppler velocities (*dark diamonds*). We can see that while the mean-subtracted (δ) intensities have a wide scatter and are very poorly correlated, the mean-subtracted Doppler velocities have a significantly tighter relationship. [See the electronic edition of the Journal for a color version of this figure.]

variation present. However, we also note that there is an apparent low-frequency period of ~ 20 minutes, “oscillation” in the line velocities. This oscillation is not consistent with the 10 minute cycle time of the instrument heaters that were being used during typical SUMER observations (see, e.g., Rybak et al. 1999). Likewise, this oscillation is also not consistent with movement of the spectrometer slit caused by its rotation compensation mechanism, which has a period of some 5 minutes. Therefore, we are left to believe that this weak periodicity in the Doppler velocities across all temperatures is solar in origin and needs further investigation that would be possible if a *TRACE* EUV time series were available.

To quantify the properties of the variation of the inferred Doppler velocities and to isolate the time and characteristic periods of variation, we have performed a wavelet transform (see Torrence & Compo 1998 for an in-depth discussion of the wavelet transform and its application) of all the emission line time series; we show an example in Figure 5. The added information gained from the wavelet transform is that we see how much power there is in the spectrum during specific time intervals. Thus, if the oscillation grows and then fades, we will see when this event happened, how long it lasted, and how much power it has, the lighter the stronger. Examination of the wavelet power spectrum of N IV in Figure 5 shows that there is no real persistent oscillation frequency but rather a collection of bursts with varying durations inside the solid black 95% “statistical significance” contours. The 20 minute oscillation discussed above is clearly identified as significant by the wavelet transform. We see, in general, that the duration of the power at any given “frequency” is only on the order of one

TABLE 2
DETAILS OF THE CORRELATION ANALYSIS OF LINE PAIRS

Line Pair	$C(I)$	$C(V)$	Lag(V)	$C^*(I)$	$C^*(V)$
N III–Ne VIII ($\lambda 770$)	0.22	0.51	2	0.46	0.76
N IV–Ne VIII ($\lambda 770$)	0.24	0.53	2	0.49	0.82
O IV–Ne VIII ($\lambda 770$)	0.21	0.46	2	0.45	0.80
O V–Ne VIII ($\lambda 770$)	0.26	0.49	1	0.51	0.81
Ne VIII ($\lambda 780$)–Ne VIII ($\lambda 770$).....	0.72	0.76	0	0.72	0.76

NOTES.—We show the intensity-intensity, $C(I)$, and velocity-velocity, $C(V)$, correlation coefficients at a time lag (number of time steps, and one time step 12.5 s) of 0. The $C(I)$ values are so small that attempts to associate a time lag between the signals is inappropriate. We use the velocities to compute the time lags. Note that using the computed velocity lags and performing the correlations again produces significantly higher values of the correlation coefficient for $C^*(V)$, while those for $C^*(I)$ are still low. The asterisk denotes that the time series have been shifted by the appropriate lag.

cycle, and thus these “events” are largely velocity bursts, not persistent periodic oscillations in velocity.

We conclude from these observations that there is a strong temporal signature for the velocities as a function of temperature with a large degree of correlation from one temperature to another. There is a small ~ 2 exposure, 25 s delay, between velocities of the cool (N III; N IV; O IV O V) lines as compared to the hotter (Ne VIII) lines. This lag time, if real, is consistent with the sound travel time between the likely formation layers of the ions. Conversely, the line intensities show an apparent physical “disconnect” between the cool lines and the hotter lines, which are effectively invariant. Therefore, it is reasonable to say that without velocity measurements, discrimination between components in the energy balance of the plasma is not practicable; line intensities, and anything derived from them (e.g., the “differential” emission measure), on their own can be misleading.

3. DISCUSSION AND FUTURE WORK

The primary objective of the observations that we have presented and analyzed in this paper was to gain a better understanding of the energy processes in, and ultimately the source of energy of, the solar corona and transition region that belongs to an elementary magnetic feature, or loop, in the atmosphere. Since we currently have no way to directly measure the energy in this region of the Sun, we must make

observations and apply them to theoretical models (see, e.g., Wikstol, Judge, & Hansteen 1998; Doyle et al. 2002; Petrie et al. 2003). Such models are based on the basic time-dependent equations of conservation of mass, momentum, and energy. The self-consistent solution of these equations for a loop requires the accurate measurement, determination, and implementation of the boundary conditions: temperature, density, velocity, turbulent velocity, and magnetic field as a function of time. These boundary conditions are applied and the solution is calculated through the loop or magnetic flux tube. The critical-free, user-determined term in these equations is the energy input, and its form is largely well-informed guesswork. Ideally, as a way forward, one could do the calculations with various energy source functions and compare the calculated values with the observed intensity, velocity, and magnetic structure. The best match of these models would provide insight into the energy source function geometry and hopefully provide a look into the physical processes.

In reality, however, one must make many assumptions to solve the equations and compare them with observations. For example, one frequently assumes the geometry of the loop is known (and easily parameterized) and does a parametric, one-dimensional solution of the mass, momentum, and energy equations. A further restriction in some calculations (see, e.g., Chae, Yun, & Poland 1997; Chae, Poland, & Aschwanden 2002) is that the time derivatives of all variables are assumed to be zero. Their simple calculation shows that in the down-flow situation, as we observe in this paper, the main energy loss is radiative, while the energy flow from above is both conductive and convective. However, even with velocities of only a few (< 10) km s $^{-1}$, convection greatly exceeds conduction in energy transported. This demonstrates, from a theoretical viewpoint, the importance of measuring and including velocity terms in studying energy balance.

Clearly, the self-consistent solution to this problem is quite difficult since, on the one hand, there are assumptions made in the model calculations, while the observations are usually, and significantly, temporal and/or spatial averages. Given the velocity variations in time that we have observed and presented above, it is not surprising that the average observations do not match even the time-dependent models. We have also seen from the observations presented above that the single loop values measured differ significantly from those of the average quiet Sun, so one must use individual loops to compare with models. While the intensity observations seem to indicate that one could use time-averaged values, this is not true for velocity. If one is to consistently model the loops anchored in the

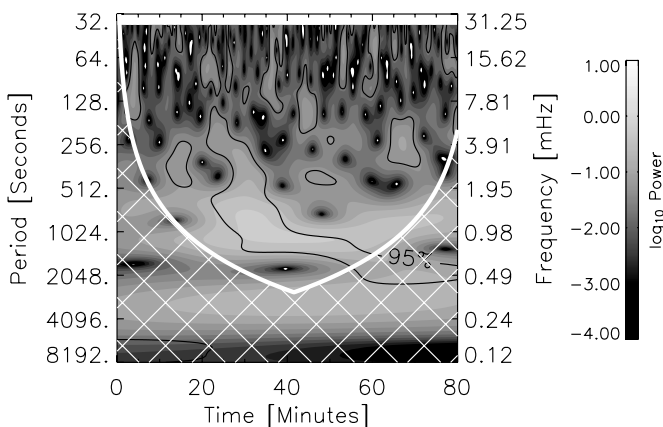


FIG. 5.—Wavelet power spectrum of the N IV ($\lambda 765.14$) Doppler velocity. This figure shows the frequency (ν) and temporal (x) variation of the power in the signal. Solid black contours outline the regions in which that signal has greater than a 95% statistical significance.

solar atmosphere, the temporal variation of velocities must be incorporated into the comparison with observations, or we will miss an essential part of the plasma's physical behavior. So, one must have good temporal and spatial resolution, including temperature and velocity, to compare with the model calculations. Such observations are rare and difficult to perform. We are currently working to obtain high spatially and temporally resolved observations over a range of temperatures of individual magnetic loops, *SOHO/TRACE* JOP 161. These data will be applied to more sophisticated models that include time variation in an attempt to deduce the energy input function.

This result will hopefully lead to a better understanding of the coronal and transition region's energy source and sustenance.

We would like to thank the anonymous referee for making some important suggestions to the text of this paper, and the SUMER (financially supported by DLR, CNES, NASA, and the ESA PRODEX program) and *TRACE* instrument teams for access to their data and for agreeing to take part in JOP 161. S. W. M. acknowledges the support of NASA's Living With A Star (LWS) Program.

REFERENCES

- Cadavid, A. C., Lawrence, J. K., Berger, T. E., & Ruzmaikin, A. 2003, *ApJ*, 586, 1409
- Chae, J., Poland, A. I., & Aschwanden, M. J. 2002, *ApJ*, 581, 726
- Chae, J., Schüle, U., & Lemaire, P. 1998a, *ApJ*, 505, 957
- Chae, J., Yun, H. S., & Poland, A. I. 1997, *ApJ*, 480, 817
- . 1998b, *ApJS*, 114, 151
- Craig, I. J. D., & Brown, J. C. 1986, *Inverse Problems in Astronomy* (London: Adam Hilger)
- Dammasch, I. E., Wilhelm, K., Curdt, W., & Hassler, D. M. 1999, *A&A*, 346, 285
- Doyle, J. G., Madjarska, M. S., Roussev, I., Teriaca, L., & Giannikakis, J. 2002, *A&A*, 396, 255
- Engvold, O., Harvey, J. W., Schrijver, C. J., & Hurlburt, N. E., ed. 2000, *Physics of the Solar Corona and Transition Region, Part I* (Dordrecht: Kluwer)
- . 2001, *Physics of the Solar Corona and Transition Region, Part II* (Dordrecht: Kluwer)
- Fleck, B., Domingo, V., & Poland, A. I. 1995, *The SOHO Mission* (Dordrecht: Kluwer)
- Handy, B. N., Acton, L. W., Kankelborg, C. C., Wolfson, C. J., & Akin, D. J., et al. 1999, *Sol. Phys.*, 187, 229
- Judge, P. G., & McIntosh, S. W. 1999, *Sol. Phys.*, 190, 331
- Judge, P. G., Tarbell, T. D., & Wilhelm, K. 2001, *ApJ*, 554, 424
- Mariska, J. T. 1992, *The Solar Transition Region* (Cambridge: Cambridge Univ. Press), chap. 6, 7
- McIntosh, S. W., Diver, D. A., Judge, P. G., Charbonneau, P., Ireland, J., & Brown, J. C. 1998, *A&AS*, 132, 145
- Petrie, G. J. D., Gontikakis, C., Dara, H. C., Tsinganos, K., & Aschwanden, M. J. 2003, *A&A*, 409, 1065
- Rybak, J., Curdt, W., Kucera, A., Schühle, U., & Wöehl, H. 1999, in *Proc. 8th SOHO Workshop, Plasma Dynamics and Diagnostics of the Solar Transition Region and Corona*, ed. J.-C. Vial & B. Kaldeich-Schürmann (ESA SP-446; Noordwijk: ESA), 579
- Sakai, J.-I., & Furusawa, K. 2002, *ApJ*, 564, 1048
- Teriaca, L. 2001, Ph.D. thesis, Queen's Univ. Belfast
- Torrence, C., & Compo, G. P. 1998, *Bull. Am. Met. Soc.*, 79, 61
- Vial, J.-C., & Kaldeich-Schürmann, B., ed. 1999, *Proc. 8th SOHO Workshop, Plasma Dynamics and Diagnostics of the Solar Transition Region and Corona* (ESA SP-446; Noordwijk: ESA)
- Wikstol, O., Judge, P. G., & Hansteen, V. H. 1998, *ApJ*, 501, 895
- Wilhelm, K., Curdt, W., Marsch, E., Schühle, U., & Lemaire, P., et al. 1995, *Sol. Phys.*, 162, 189